Control-Integrated Design by Theoretical Simulation for a Torque-Actuated 6-SBU Stewart Platform

Biswajit Halder[*], Rana Saha[#], and Dipankar Sanyal[+]
Department of Mechanical Engineering, Jadavpur University, Kolkata, India
[*]biswajeeet@gmail.com, [#]rsaha@mech.jdvu.ac.in, [+]dsanyal@mech.jdvu.ac.in

***Abstract*—A design algorithm has been proposed for a Stewart platform with six legs, each having a ball-screw at the middle and powered by a torque motor at the bottom. When a motor shaft rotates, the leg extends or collapses and the axis could rotate about a spherical joint supporting the motor. Consequent actuation from all the legs through a universal joint at the top of each causes the platform to change its pose. The joints at each end lie on the intersection of a pitch circle and a semi-regular hexagon. An inverse model that neglects friction and leg inertia has been employed in a step-by-step simultaneous search to determine the platform height at the neutral and the radius of the bottom pitch circle within the constraint of permissible joint angle and motor specifications. The proposed control for a basic pose demand involves a feedforward estimation of motor torque variation, a proportional-derivative feedback and appropriate compensating demand for minimizing unwanted coupled motion. The forward modeling of the pose dynamics and its Simulink implementation have established the control as satisfactory.**

***Index Terms*—feedforward-feedback, forward modeling, inverse modeling, parallel manipulator, Simulink**

I. Introduction

Parallel manipulators are widely used as laboratory-scale flight or ship-motion simulators for assessing stability and control performance of certain on-board systems subjected to complex inertial loading. Any such manipulator has integrated control for imparting a range of desired motions to a large payload within a small workspace. In order to take care of the imprecision related to a number of passive joints in the system and multiplicity of the response to a definite command, the control is critical. A Stewart platform [1] is the most popular parallel manipulator with six degrees-of-freedom.

A Stewart platform involves six linearly extensible legs with active electric or hydraulic drive for each. In a conventional Stewart platform, the bottom end of each leg is connected by a spherical or universal joint to a stationary frame at the bottom and the top end is connected by a spherical joint to the moving platform that supports a payload on top. Legs only with prismatic joints between its upper and lower parts have been analyzed in the past, though nowadays various laboratories are exploring the use of ball-screw joints. Both 6-SPS and 6-UPS configurations have been extensively analyzed [2-6],where 6 stands for the number of joints of same type, the first alphabet S or U corresponds to spherical or universal joint with the fixed frame at one end of each leg, P refers to the prismatic joint within each leg and the last alphabet S implies spherical joint with the moving platform at the other end. Joints at the bottom and at the top are usually arranged along the vertices of two regular [3] or semi-regular hexagons [2, 4, 5]. Merlet [3] considered 3/6 configuration, in which one of the ends of two legs terminated to a common bi-spherical joint, each located at the vertex of an equilateral triangle. Controlling the input to each leg is necessary, causing its length to change, with the objective of carrying the top platform through desired position and orientation, together called the pose.

Liu et al. [2] and Merlet [3] modeled both the forward and inverse kinematics of a Stewart platform and proposed simplified solution schemes for the forward kinematics. While the inverse kinematics deals with estimating the neutral length and stroke of the legs from the specified range of desired platform pose, the forward or direct kinematics are meant for control analysis for predicting the platform pose from the known length of the legs. An ingenious solution scheme is necessary for the forward dynamics problem to guide the mechanism through any desired instantaneous solution among the possible multiple solutions for an intermediate pose [7].

Fichter [4] neglected the effect of leg inertia to obtain a simple forward dynamics model based on Newton-Eulerian approach for computing actuating forces on a Stewart platform corresponding to input of actuation forces to the legs. Employing Newton-Eulerian analysis, Dasgupta and Mrithyunjaya [5, 6] arrived at both inverse and forward models for the kinematics and dynamics. Their prediction showed the effectiveness of a PD control for the force inputs to the legs corresponding to different pose dynamics, with the control estimated from the difference between the required and the predicted leg lengths at each instant of time. Sensors like LVDT is necessary to measure the instantaneous length of each leg in order to implement the internal control of correcting the leg length leaving the pose control to be taken care of in an outer loop. A similar PD control strategy is implemented using feedback of actuator length [8].

Recently, Andreff and Martinet [9] used a classical perspective camera as an additional contactless sensor for constructing the platform pose directly and developed a control-devoted projective kinematic model. In their integrated approach of designing the vision-control robot in the form of Stewart platform, both the internal and external control loops have been considered together.

DOI: 01.IJMMS.02.02.51

Thus, the problem of multiple solutions of the forward dynamics was overcome through additional sensor measurements. Tahri et al. [10] employed a central omni-directional camera suitable for high-speed task.

Design of a Stewart platform driven by controlled torque input from a variable-speed DC motor to each of the six legs with ball-screw joints has been reported here. Such a motor drive has been chosen in view of the commercial availability of brushless DC motors and proven control performance of each with simple PID feedback. The active rotation of each leg about the motor axis has been considered in the modeling that did not arise in the earlier analyses with prismatic legs. Both the inverse and forward models of the chosen arrangement shown in Fig. 1 have been developed and implemented in Matlab-Simulink frame leading to the control-integrated design of the mechanism as a mechatronic system.

The main objective of the proposed control design is to obtain a control structure with minimal cross-coupled motion over the demanded basic motion in surge, sway, heave, roll or pitch. A thorough design analysis for the selection of the appropriate actuators has been accomplished in association with optimizing the platform dimensions. Also, a control strategy along with control gains has been carried out. Of course posing of compensating demands for reducing the unwanted cross-coupled motion is a notable feature of the control strategy involving proportional and derivative feedbacks and feedforward.

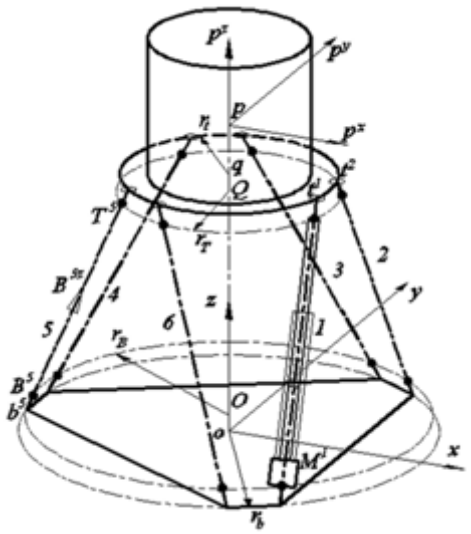

Figure 1. Schematic of a Stewart Platform at Neutral Pose

II. Platform Configuration

Figure 1 shows the schematic of a Stewart platform supporting a cylindrical payload on top of a circular disc with center at Point q and radius r_t. However, the center of mass of the payload together with the disc lies at Point p. Below the disc, there are six actuation systems i = 1 to 6. From the top towards the bottom, each system has a cylindrical stub, a universal joint, a leg comprising of upper and lower parts, a motor, a spherical joint and another cylindrical stub. Fig. 1 shows System 1 in relatively greater detail with the motor indicated as M^1, while in System 5 Points b^5, B^5, T^5 and t^5 mark the extent of the bottom stub, the leg and the top stub respectively. While T^5 represents the universal joint and B^5 the spherical joint, B^{5z} shows the leg axis. For the other five leg systems, the respective centerlines 1 to 4 and 6 represent the axes and filled circles the joints.

While the stubs on the top terminate at the points shown by unfilled dishes at the periphery of the disc, the bottom stubs end at a semi-regular hexagonal frame with circumscribing circle of radius r_b and the center at o. The frame fixes the mechanism on the ground. The open dishes at the disc periphery also lie at the vertices of another semi-regular hexagon.

While the universal joints T^i lie on a circle of radius r_T with center at Q, the spherical joints B^i lie on a circle of radius r with center at O. In the stationary and moving coordinate systems with origins shownat Points o and p respectively and the axes denoted by (x,y,z) and (p^x,p^y,p^z) respectively, the angular locations for Points $b^i$and t^i can be expressed as

$$\left.\begin{aligned}
&\theta_{b1(o)} = \theta_s - (\pi/3);\ \theta_{b2(o)} = (\pi/3) - \theta_s;\\
&\theta_{t1(p)} = -\theta_s;\ \theta_{t2(p)} = \theta_s;\\
&\theta_{bi(o)} = \theta_{b1(o)} + (i-1)\pi/3 \quad \text{for } i = 3 \text{ and } 5;\\
&\theta_{bi(o)} = \theta_{b2(o)} + (i-1)\pi/3 \quad \text{for } i = 4 \text{ and } 6;\\
&\theta_{ti(p)} = \theta_{t1(p)} + (i-1)\pi/3 \quad \text{for } i = 3 \text{ and } 5;\\
&\theta_{ti(p)} = \theta_{t2(p)} + (i-1)\pi/3 \quad \text{for } i = 4 \text{ and } 6;
\end{aligned}\right\}, \quad (1)$$

where a letter outside and within parentheses in the subscript respectively identify a point and the origin or the axis direction of the coordinate system for the associated variable and half of $\angle t^1 q t^2$ is written as q_s. At the neutral pose described in Fig. 1, Line $oOQqp$ is vertical and the axis of each leg is collinear to its end stubs. The running length of the i^{th} leg system can be determined as

$$L_i = l_i^t + l_i^b + l_i^a, \quad (2a)$$

where superscript t, b and a to a variable stands for the top, bottom and actuated part of a leg. Particularly, at the neutral pose, indicated by a 0 in the subscript, axes of these parts are collinear. In other words, the running length at the neutral is equal to the distance of point b^i and t^i. Therefore, expressing the coordinate of a point by a vector $\mathbf{x}$, it can be written that

$$L_{i0} = \left|\mathbf{x}_{bi(o)} - \mathbf{x}_{ti(o)}\right|. \quad (2b)$$

The angular locations for Points B^i and for Points T^i in the stationary and the moving coordinates can be expressed as

$$\left.\begin{aligned}
&\theta_{Ti(p)} = \theta_{ti(p)} + (\theta_{bi(o)} - \theta_{ti(p)})(L_{i0} - l_i^t)/L_{i0},\ i = 1 \text{ to } 6\\
&\text{and}\\
&\theta_{Bi(o)} = \theta_{bi(o)} + (\theta_{bi(o)} - \theta_{ti(p)})l_i^b/L_{i0})/L_{i0},\ i = 1 \text{ to } 6
\end{aligned}\right\}. \quad (3)$$

DOI: 01.IJMMS.02.02.51

In terms of these angles and the height of Points *p* and *q* above Point *o* at the neutral pose written as $z_{p0(o)}$ and $z_{q0(o)}$ respectively, the coordinates of points b^i, B^i, T^i and t^i can be written as

$$\mathbf{x}_{bi(o)} = \begin{pmatrix} r_b \cos\theta_{ti(o)} & r_b \sin\theta_{ti(o)} & 0 \end{pmatrix}^T, \quad (4a)$$

$$\mathbf{x}_{Bi(o)} = \begin{pmatrix} r_B \cos\theta_{Bi(o)} & r_B \sin\theta_{Bi(o)} & \dfrac{z_{q0(o)} \times L_i^b}{L_{i0}} \end{pmatrix}^T, \quad (4b)$$

$$\mathbf{x}_{Ti(o)} = \begin{pmatrix} r_T \cos\theta_{Ti(o)} & r_T \sin\theta_{Ti(o)} & \dfrac{z_{q0(o)}\left(L_{i0} - l_i^t\right)}{L_{i0}} - z_{p0(o)} \end{pmatrix}^T \quad (4c)$$

and

$$\mathbf{x}_{ti(p)} = \begin{pmatrix} r_t \cos\theta_{ti(p)} & r_t \sin\theta_{ti(p)} & z_{q0(o)} - z_{p0(o)} \end{pmatrix}^T. \quad (4d)$$

Each leg in Fig. 1 has been chosen as a ball-screw joint. The lower part of the joint could be rotated by the motor coupled to it and the top part could extend or retract depending on the direction of motor rotation. Of course, the rates and directions of the motor rotations together decide what type of motion the payload would undertake. This motion initiated from the neutral could be a pure translation or a pure rotation. While, the translations along *x*, *y* and *z* axes, respectively referred as surge (Su), sway (Sw) and heave (H), describe the position acquired by Point *p* on the payload as

$$\mathbf{x}_{p(o)} = \begin{pmatrix} x & y & z_{p0(o)} + z \end{pmatrix}^T, \quad (5a)$$

any rotational motion about *x*, *y* and *z* axes, respectively called roll (R), pitch (P) and yaw (Y), provides the orientation of the payload as

$$\boldsymbol{\theta}_{(o)}^{p} = \begin{pmatrix} \alpha & \beta & \lambda \end{pmatrix}^T. \quad (5b)$$

The direction B^{5z} along which the translation of the upper part of Leg 5 would take place has also been indicated in Fig. 1. Thus for any motorized leg *i*, B^{iz} is the direction along which the leg length changes due to active motor rotation causing motion of T^i relative to B^i. Accepting the direction B^{iy} as the axis of rotation of the leg centerline, six rotating coordinate systems (B^{ix},B^{iy},B^{iz}) are defined with origins at the stationary points B^i. For any pose away from the neutral, the axes of the stubs and the leg of each actuation system does not remain collinear.

Of course, the bottom stubs and Points *o* and *O* are stationary. However, the axis B^{iz} of each leg could rotate about the spherical joint at B^i, causing angular deviation between the axes of the bottom stub and the leg. Consequent to all these rotations along with the translations of the upper parts of the legs, Points T^i, t^i, *Q*, *q* and *p* would move. The universal joint at each of T^i permits the deviation between the axes of each leg and the associated top stub, as necessitated to sustain the desired payload motion.

Only for pure yawing motion from the neutral, Points *p*, *q* and *Q* would remain stationary. For this case and the case of pure heaving motion, the directions of axes p^z and *z* remain coincident and the circles with Points T^i and t^i at the periphery would remain horizontal. The top stubs joining the respective peripheral points would undergo pure vertical motion during heaving and pure angular rotation during yawing. This angular motion is obviously equal to that of the payload about *z*-axis. The spherical joint permits this rotation. In the set-up being investigated, such joints have been considered at the bottom of each leg that would cause each leg to rotate passively also by the same amount. This yields a 6-SBU joint configuration, where B refers to the ball-screw joint replacing P for the conventional prismatic joint [5]. This configuration has been taken up for the subsequent kinematic and dynamic modeling.

III. Inverse Kinematic Modeling

An objective of the inverse kinematic modeling is to express the lengths of the six legs in terms of the pose. When the mechanism is subjected to a pure surge, sway or heave, both the stationary and the moving coordinate systems remain parallel to each other and the corresponding component of the unit vectors $\hat{\mathbf{e}}_O$ and $\hat{\mathbf{e}}_p$ in these systems remain identical throughout the motion. It is conventional to describe a general angular motion as an ordered combination of roll, pitch and yaw. For any such motion, the two coordinate systems do not remain parallel any more. For a payload pose, the unit vectors

$$\hat{\mathbf{e}}_p = (\hat{i}_p \quad \hat{j}_p \quad \hat{k}_p)^T, \quad (6a)$$

and

$$\hat{\mathbf{e}}_O = (\hat{i} \quad \hat{j} \quad \hat{k})^T, \quad (6b)$$

can be related through the rotation matrix $\mathbf{R}_{p,o}$ for transforming a vector from the moving to stationary coordinate system [11] as

$$\hat{\mathbf{e}}_p = \mathbf{R}_{p,o}\hat{\mathbf{e}}_O, \quad (6c)$$

where

$$\mathbf{R}_{p,o} = \begin{bmatrix} i_{(px)} & i_{(py)} & i_{(pz)} \\ j_{(px)} & j_{(py)} & j_{(pz)} \\ k_{(px)} & k_{(py)} & k_{(pz)} \end{bmatrix}, \quad (6d)$$

with

$$\left.\begin{aligned} &i_{(px)} = \cos\beta\cos\gamma;\ i_{(py)} = \sin\alpha\sin\beta\cos\gamma + \cos\alpha\sin\gamma; \\ &i_{(pz)} = -\cos\alpha\sin\beta\cos\gamma + \sin\alpha\sin\gamma; \\ &j_{(px)} = -\cos\beta\sin\gamma;\ j_{(py)} = -\sin\alpha\sin\beta\sin\gamma + \cos\alpha\cos\gamma; \\ &j_{(pz)} = -\cos\alpha\sin\beta\sin\gamma + \sin\alpha\cos\gamma; \\ &k_{(px)} = \sin\beta;\ k_{(py)} = -\sin\alpha\cos\beta;\ k_{(pz)} = \cos\alpha\cos\beta. \end{aligned}\right\} \quad (6e)$$

DOI: 01.IJMMS.02.02.51

Now, (4c), (4d), (5a) and (6c) yield the coordinates of T^i and t^i as

$$\mathbf{x}_{Ti(o)} = \mathbf{x}_{p(o)} + \mathbf{R}^T_{p,o}\mathbf{x}_{Ti(p)}, \quad (7a)$$

and

$$\mathbf{x}_{ti(o)} = \mathbf{x}_{p(o)} + \mathbf{R}^T_{p,o}\mathbf{x}_{ti(p)}. \quad (7b)$$

Hence, from (4a), (4b), (7a) and (7b), the fixed lengths of the i^{th} top and bottom stubs, the instantaneous length of the i^{th} leg and the unit vectors along these can be determined as

$$l^t_i = |\mathbf{x}_{ti(o)} - \mathbf{x}_{Ti(o)}|, \quad (8a)$$

$$l^b_i = |\mathbf{x}_{Bi(o)} - \mathbf{x}_{bi(o)}|, \quad (8b)$$

$$l^a_i = |\mathbf{x}_{Ti(o)} - \mathbf{x}_{Bi(o)}|, \quad (8c)$$

$$\hat{\mathbf{e}}_{tTi} = (\mathbf{x}_{ti(o)} - \mathbf{x}_{Ti(o)})/|\mathbf{x}_{ti(o)} - \mathbf{x}_{Ti(o)}|, \quad (8d)$$

$$\hat{\mathbf{e}}_{Bbi} = (\mathbf{x}_{Bi(o)} - \mathbf{x}_{bi(o)})/|\mathbf{x}_{Bi(o)} - \mathbf{x}_{bi(o)}|, \quad (8e)$$

and

$$\hat{k}_{Bi} = (\mathbf{x}_{Ti(o)} - \mathbf{x}_{Bi(o)})/|\mathbf{x}_{Ti(o)} - \mathbf{x}_{Bi(o)}|. \quad (8f)$$

There is a physical constraint on the maximum permissible angle that a class of joint allows between its members. Therefore, for the most demanding poses of the payload, the angles should be estimated at the spherical and the universal joints between the axes of a leg and its associated bottom and top stubs. These angles can be found out as

$$\lambda_{Ti} = \cos^{-1}(\hat{\mathbf{e}}_{tTi}\hat{k}_{Bi}), \quad (9a)$$

and

$$\lambda_{Bi} = \cos^{-1}(\hat{\mathbf{e}}_{Bbi}\hat{k}_{Bi}). \quad (9b)$$

It is also imperative to estimate the motor capacity in terms of velocity and the acceleration demands arising from the desired payload poses. Using notations as explained in the context of (1) and (2a), the linear and angular velocities and the linear and angular accelerations of the payload can be expressed respectively as

$$\left.\begin{aligned} \mathbf{v}_{p(o)} &= (v_{p(x)} \quad v_{p(y)} \quad v_{p(z)})^T \\ \boldsymbol{\omega}^p_{(o)} &= (\omega^p_{(x)} \quad \omega^p_{(y)} \quad \omega^p_{(z)})^T \\ \mathbf{a}_{p(o)} &= (a_{p(x)} \quad a_{p(y)} \quad a_{p(z)})^T \\ \boldsymbol{\alpha}^p_{(o)} &= (\alpha^p_{(x)} \quad \alpha^p_{(y)} \quad \alpha^p_{(z)})^T \end{aligned}\right\}, \quad (10)$$

that in combination with (6c) yields

$$\mathbf{v}_{p(p)} = (v_{p(px)} \quad v_{p(py)} \quad v_{p(pz)})^T = \mathbf{R}_{p,o}\mathbf{v}_{p(o)}, \quad (11a)$$

$$\boldsymbol{\omega}^p_{(p)} = (\omega^p_{(px)} \quad \omega^p_{(py)} \quad \omega^p_{(pz)})^T = \mathbf{R}_{p,o}\boldsymbol{\omega}^p_{(o)}, \quad (11b)$$

$$\mathbf{a}_{p(p)} = (a_{p(px)} \quad a_{p(py)} \quad a_{p(pz)})^T = \mathbf{R}_{p,o}\mathbf{a}_{p(o)}, \quad (11c)$$

and

$$\boldsymbol{\alpha}^p_{(p)} = (\alpha^p_{(px)} \quad \alpha^p_{(py)} \quad \alpha^p_{(pz)})^T = \mathbf{R}_{p,o}\boldsymbol{\alpha}^p_{(o)}. \quad (11d)$$

The velocity of Point T^i can then be obtained by using (4c), (11a) and (11b) as

$$\mathbf{v}_{Ti(o)} = \mathbf{R}^T_{p,o}\{\mathbf{v}_{p(p)} + \boldsymbol{\omega}^p_{(p)} \times \mathbf{x}_{Ti(p)}\}, \quad (12a)$$

and

$$\mathbf{a}_{Ti(o)} = \mathbf{R}^T_{p,o}\{\mathbf{a}_{p(p)} + \boldsymbol{\alpha}^p_{(p)} \times \mathbf{x}_{Ti(p)} + 2\boldsymbol{\omega}^p_{(p)} \times \mathbf{v}_{Ti(p)}\}. \quad (12b)$$

The velocity and acceleration given by (12a) and (12b) can be used to determine the velocity and acceleration of Points T^i in the rotating coordinate system for each actuator as

$$\mathbf{v}_{Ti(Bi)} = \mathbf{R}^T_{Bi,o}\mathbf{v}_{Ti(o)}, \quad (13a)$$

and

$$\mathbf{a}_{Ti(Bi)} = \mathbf{R}^T_{Bi,o}\mathbf{a}_{Ti(o)}. \quad (13b)$$

where the rotational matrix

$$\mathbf{R}_{Bi,o} = \begin{bmatrix} i_{(Bix)} & i_{(Biy)} & i_{(Biz)} \\ j_{(Bix)} & j_{(Biy)} & j_{(Biz)} \\ k_{(Bix)} & k_{(Biy)} & k_{(Biz)} \end{bmatrix}, \quad (14a)$$

that couples the unit vector for the i^{th} rotating coordinate system defined as

$$\hat{\mathbf{e}}_{Bi} = (\hat{i}_{Bi} \quad \hat{j}_{Bi} \quad \hat{k}_{Bi})^T, \quad (14b)$$

with that in the stationary coordinate system by the relation

$$\hat{\mathbf{e}}_{Bi} = \mathbf{R}_{Bi,o}\hat{\mathbf{e}}_o, \quad (14c)$$

$\hat{k}_{Bi}$ in (14b) defined by (8f) and the other two unit vectors in (14b) obtained as

$$\hat{j}_{Bi} = \hat{k}_{Bi} \times \mathbf{v}_{Ti(o)}/|\hat{k}_{Bi} \times \mathbf{v}_{Ti(o)}| \text{ for } \mathbf{v}_{Ti(o)} \neq 0, \quad (14d)$$

or

$$\hat{j}_{Bi} = \hat{k}_{Bi} \times \hat{k}'/|\hat{k}_{Bi} \times \hat{k}| \text{ for } \mathbf{v}_{Ti(o)} = 0, \quad (14e)$$

and

$$\hat{i}_{Bi} = \hat{j}_{Bi} \times \hat{k}_{Bi}, \quad (14f)$$

along with the scalars in (14a) defined as

$$\left.\begin{aligned} i_{(Bix)} &= \hat{i}_{Bi}.\hat{i}; \; i_{(Biy)} = \hat{i}_{Bi}.\hat{j}; \; i_{(Biz)} = \hat{i}_{Bi}.\hat{k}; \\ j_{(Bix)} &= \hat{j}_{Bi}.\hat{i}; \; j_{(Biy)} = \hat{j}_{Bi}.\hat{j}; \; j_{(Biz)} = \hat{j}_{Bi}.\hat{k}; \\ k_{(Bix)} &= \hat{k}_{Bi}.\hat{i}; \; k_{(Biy)} = \hat{k}_{Bi}.\hat{j}; \; k_{(Biz)} = \hat{k}_{Bi}.\hat{k}, \end{aligned}\right\}. \quad (14g)$$

It is evident that (14d) and (14f) have been defined so as to capture the velocity of i^{th} leg in the plane $B^{iz}B^{ix}$. Since the upper part across the ball-screw joint has a universal joint at the top and the lower part has a spherical joint at the bottom, the motion of a leg can be described as follows. The first and second rates of extension of the actuated leg correspond respectively to the component of the linear velocity and acceleration of the top joint along the screw axis. Of course, the other nonzero component of the linear velocity and

DOI: 01.IJMMS.02.02.51

acceleration along B^{ix} direction correspond to the angular motion of the screw axis. In fact, the upper part and the motor platform do not have any relative angular motion. These components acquire the same swing velocity $\omega^{ui}_{(Biy)}$ and acceleration $\alpha^{ui}_{(Biy)}$ about the direction B^{iy} and about the screw axis B^{iz}, the components undergo passive motion with rotational velocity $\omega^{ui}_{(Biz)}$ and acceleration $\alpha^{ui}_{(Biz)}$ that are equal to the respective components of the payload rotation about the screw axis. Of course the extension rates of the leg are provided by the rotation of the lower part relative to the upper part of the screw joint with pitch p^b. Thus for the i^{th} leg, using superscripts *mi*, *ui* and *li* respectively for the motor and the upper and lower parts of the screw joint, it can be written that

$$\dot{l}_i^a = v^{ui}_{(Biz)} = \mathbf{v}_{Ti(Bi)} \cdot \hat{k}_{Bi}, \tag{15a}$$

$$\ddot{l}_i^a = a^{ui}_{(Biz)} = \mathbf{a}_{Ti(Bi)} \cdot \hat{k}_{Bi}, \tag{15b}$$

$$\boldsymbol{\omega}^{mi}_{(Bi)} = \boldsymbol{\omega}^{ui}_{(Bi)} = \omega^{ui}_{(Biy)} \hat{j}_{Bi} + \omega^{ui}_{(Biz)} \hat{k}_{Bi}, \tag{15c}$$

$$\boldsymbol{\omega}^{li}_{(Bi)} = \boldsymbol{\omega}^{ui}_{(Bi)} + (\dot{l}_i^a / p^b) \hat{k}_{Bi}, \tag{15d}$$

$$\boldsymbol{\alpha}^{mi}_{(Bi)} = \boldsymbol{\alpha}^{ui}_{(Bi)} = \alpha^{ui}_{(Bix)} \hat{i}_{Bi} + \alpha^{ui}_{(Biy)} \hat{j}_{Bi} + \alpha^{ui}_{(Biz)} \hat{k}_{Bi}, \tag{15e}$$

and

$$\boldsymbol{\alpha}^{li}_{(Bi)} = \boldsymbol{\alpha}^{ui}_{(Bi)} + (\ddot{l}_i^a / p^b) \hat{k}_{Bi}, \tag{15f}$$

where the component in (15c) to (15f) can be expressed as

$$\left.\begin{aligned} \omega^{ui}_{(Biy)} &= v_{Ti(Bix)} / \dot{l}_i^a; \\ \omega^{ui}_{(Biz)} &= k_{(Bix)} \omega^p_{(x)} + k_{(Biy)} \omega^p_{(y)} + k_{(Biz)} \omega^p_{(z)}; \\ \alpha^{ui}_{(Bix)} &= -\mathbf{a}_{Ti(Bi)} \cdot \hat{j}_{Bi} / \dot{l}_i^a; \; \alpha^{ui}_{(Biy)} = \mathbf{a}_{Ti(Bi)} \hat{i}_{Bi} / \dot{l}_i^a \\ \alpha^{ui}_{(Biz)} &= k_{(Bix)} \alpha^p_{(x)} + k_{(Biy)} \alpha^p_{(y)} + k_{(Biz)} \alpha^p_{(z)}. \end{aligned}\right\} \tag{15g}$$

Equation (15a) provides the estimates of instantaneous lengths l_i^a of all the legs with motorized actuation. Desired lengths of the legs at the extremes can be found out from these estimates obtained corresponding to the entire range of desired output motion of the platform.

IV. Inverse Dynamic Modeling

The inverse model provides a way to estimate the actuation input of current to the coils of the torque motors necessary for achieving the desired payload motion. In addition to the motor-torque induced axial actuating force, to be estimated, is $F^e_{Ti(Biz)}$ on the upper part of the i^{th} screw joint acting along the screw axis, the upper part receives a transverse force $F_{Ti(Bix)}$ as well due to the weight, friction and inertia forces corresponding to the rotation of the screw-joint axis about Point B^i.

For the payload together with the disc with combined mass m^p and the centroidal moment of inertia $I^p_{(px)}$, $I^p_{(py)}$ and $I^p_{(pz)}$, the equations of dynamics in the coordinate system with origin at Point *p* shown in Fig. 1 can now be written as

$$\sum_{i=1}^{6} \left\{ \hat{k}_{Bi} F^e_{Ti(Biz)} + \boldsymbol{F}_{Ti(Bix)} \right\} = m^p \left(a_{p(o)} + g\hat{k} \right), \tag{16a}$$

$$\sum_{i=1}^{6} \mathbf{x}_{Ti(p)} \times \left\{ \hat{k}_{Bi} F^e_{Ti(Biz)} + \boldsymbol{F}_{Ti(Bix)} \right\} = \mathbf{I}^p_{(p)} \boldsymbol{\alpha}^p_{(p)} + \mathbf{P}, \tag{16b}$$

with

$$\mathbf{I}^p_{(p)} = diag\left(I^p_{(px)} \quad I^p_{(py)} \quad I^p_{(pz)} \right), \tag{16c}$$

and

$$\mathbf{P} = \begin{bmatrix} \left(I^p_{(py)} - I^p_{(pz)} \right) \omega^p_{py} \omega^p_{pz} \\ \left(I^p_{(pz)} - I^p_{(px)} \right) \omega^p_{pz} \omega^p_{px} \\ \left(I^p_{(px)} - I^p_{(py)} \right) \omega^p_{px} \omega^p_{py} \end{bmatrix} \hat{e}_p \tag{16d}$$

By neglecting the transverse force component, one can solve the above equations simultaneously with known description of the right-hand sides, so as to make an estimate of the required forces $F^e_{Ti(Biz)}$ from motors.

V. Configuration Design of a Stewart Platform

Sections 2 to 4 provide the equations for the length, velocity, force and joint angles pertaining to the legs of the mechanism depicted in Fig. 1 for a specified range of the basic displacements of a payload. The specifications have been taken as ±0.3 m surge, sway and heave, $\pm 15^0$ roll and $\pm 10^0$ pitch and yaw for a 100 kg payload along with the maximum limits for the rates given as ±0.05 m/s, $\pm 12.6^0$/s, 0.05 m/s^2 and 100^0/s^2. Of course, deciding a suitable diameter for the disc that would support the payload of a given size is the starting point of the design. The diameter of the disc, the lengths of the top and bottom stubs and $\angle t^1 q t^2$ have been assumed to be equal to 0.5mm, 0.1m and 0.04m and 10^0 respectively. The design objective has been posed as estimating the feasible combination of $z_{p0(o)}$, the neutral height of the disc from the base and r_b, the base radius.

DOI: 01.IJMMS.02.02.51

In order to carry out the design, each basic motions has been applied such that the payload displacement from one end to the another in the specified range takes place in the shortest possible time for the specified limits of the velocity and the acceleration. Danaher Motion EC2-B23-10L-05B actuators with 0.45m and 0.6m strokes have been considered, since the desired heaving by 0.6m demands a change of actuated length of about 0.6m. A maximum joint angle, λ_{max} = 20^0 has been considered as a design constraint for both the spherical and universal joints. Since the bottom joint angle has never been found to be more than the top one, only the top limit has been shown in Figs. 2 and 3.

Two more design constraints L_{min} and L_{max} are used for the minimum and maximum running lengths limits respectively, estimated by (2) for an actuator at the minimum and maximum strokes. The lower constraining lengths have been taken as 1.18m and 1.286m for the actuators with 0.45m and 0.6m stroke respectively and the corresponding upper constraining length for each has been obtained by adding the respective stroke.

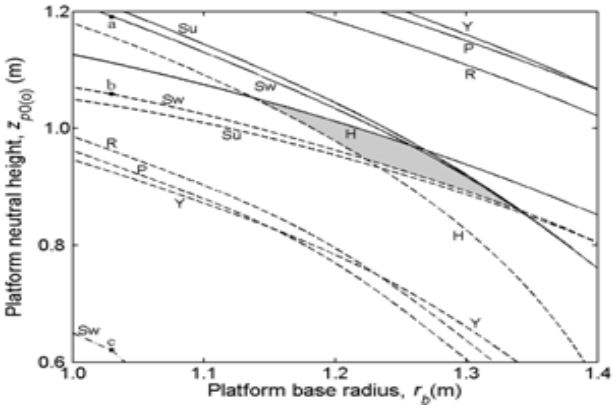

Figure2. Variation of limiting height-radius pair of platform shown by solid, dashed and dash-dot lines respectively at the limits of maximum stroke, minimum stroke and maximum joint angle along with the admissible zone indicated in shade for achieving prescribed 6 DOF motion by Danaher-motion EC2-B23-10L-05B-450.

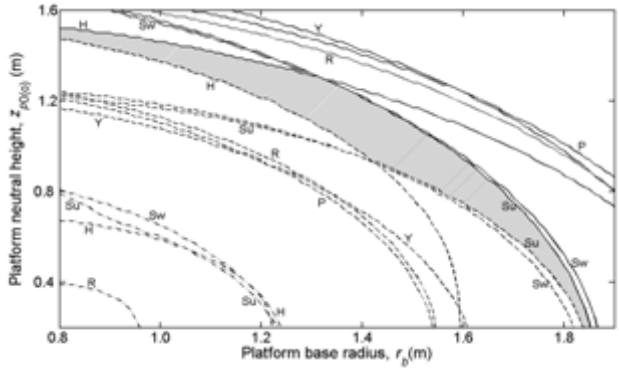

Figure3. Variation of limiting height-radius pair of platform shown by solid, dashed and dash-dot lines respectively at the limits of maximum stroke, minimum stroke and maximum joint angle along with the admissible zone indicated in shade for achieving prescribed 6 DOF motion by Danaher-motion EC2-B23-10L-05B-600.

The admissibility check to determine the limiting curve corresponding to each constraint has been carried out by varying only one of the values of $z_{p0(o)}$ or r_b at a time in 0.01m step.

Out of the total set of values of $z_{p0(o)}$ and r_b, nth value of $z_{p0(o)}$ and mth value of r_b can be represented by $z^n_{p0(o)}$ and r_b^m respectively which yields three limiting values-

$l^{max}_{a(m,n)}$ as maximum actuated length,

$l^{min}_{a(m,n)}$ as minimum actuated length and

$\lambda^{max}_{T(m,n)}$ as maximum top joint angle.

The values are represented by the following expressions:

$$l^i_{a(m,n)} = f_1\left(r_b^m, z^n_{p0(o)}\right), \tag{17}$$

$$\lambda_{Ti(m,n)} = f_2\left(r_b^m, z^n_{p0(o)}\right), \tag{18}$$

$$l^{max}_{a(m,n)} = \max_i\left(\max_{\Omega}\left\|l^i_{a(m,n)}\right\|_2\right), \tag{19a}$$

$$l^{min}_{a(m,n)} = \min_i\left(\min_{\Omega}\left\|l^i_{a(m,n)}\right\|_2\right), \tag{19b}$$

$$\lambda^{max}_{T(m,n)} = \max_i\left(\max_{\Omega}\left\|\lambda_{Ti(m,n)}\right\|_2\right), \tag{19c}$$

where

$$\Omega = (x, y, z, \alpha, \beta, \gamma)^T, \tag{20}$$

$$L_{max} > l^t + l^b + l^{max}_{a(m,n)}, \tag{21a}$$

$$L_{min} < l^t + l^b + l^{min}_{a(m,n)}, \tag{21b}$$

$$\lambda_{max} > \lambda^{max}_{T(m,n)}, \tag{21c}$$

Designing for the case of sway may be taken up for a sample illustration. For a chosen value of r_b equal to 1.03m in Fig. 2, $z_{p0(o)}$ variation from 0.6m to 1.2m in 0.01m step may be considered. Points a, b and c corresponds to 1.19m, 1.06m and 0.62m respectively. It is evident that for any value of $z_{p0(o)}$ below a and above both b and c are admissible from the viewpoints of maximum limiting stroke, minimum limiting stroke and maximum joint angle respectively. In fact, the figure clearly reveals that any design in the range of $z_{p0(o)}$ between Points a and b for r_b qual to 1.03m would support all the displacement variations excepting heave.

The region shown by hatched lines within the limiting curves corresponding to maximum and minimum strokes for heave and sway displacements satisfies all the design objectives and constraints. Some of the limiting joint angle lines do not appear in Figs. 2 and 3 for being confined to region bounded by lower platform height and smaller bottom-circle radius than shown in the figures. Any value of the variable less than those on the solid lines and greater than those on the other two line types indicates admissible values corresponding to the constraint that a particular line type represents. The variable pair prior to any step change that made an admissible design inadmissible has been shown as a point on a limiting line. It is apparent from Fig. 2 that the actuator with 0.45m stroke has a very narrow region of

DOI: 01.IJMMS.02.02.51

admissible design around $z_{p0(o)}$ and r_b respectively equal to 0.95m 1.25m, whereas Fig. 3 shows that the actuator with 0.6m stroke has a much wider region around 1.4m and 1.1m respectively. Hence, the dynamic admissibility test depicted in Fig. 4 has been carried out only for the latter actuator.

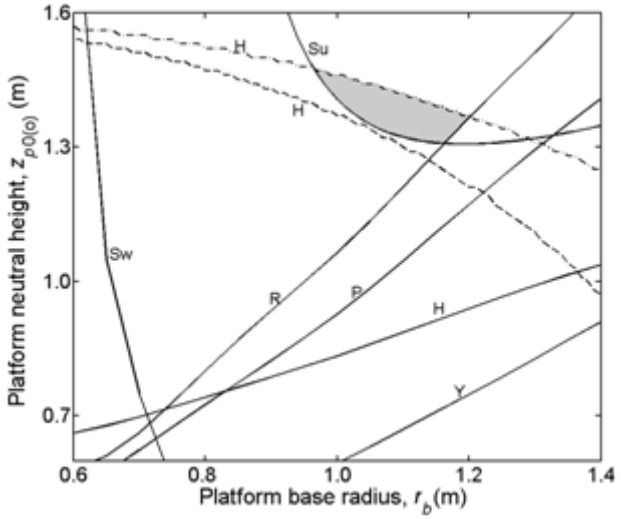

Figure 4. Variation of limiting height-radius pair of platform shown by solid, dashed and dash-dot lines respectively at the limits of peak force, minimum heave and maximum heave along with the admissible zone indicated in shade for achieving prescribed 6 DOF motion by Danaher-motion EC2-B23-10L-05B-600.

Figure 4 depicts the dynamically admissibility of the design corresponding to the 100% duty-cycle force limit constraint of 830 N available in case of Danahaer-motion EC2-B23-10L-5B-600 actuator along with keeping 7% margin for friction and another 20% for other factors. In this figure, the critical cases of the kinematic-constraint admissibility zone have also been plotted. It is evident that r_b and $z_{p0(o)}$ respectively equal to 1100 mm and 1400 mm provide an acceptable design solution. The corresponding minimum, neutral and the maximum actuated lengths are 1286 mm, 1647 mm and 1886 mm respectively. It may be mentioned at this stage that the effect of the transverse inertial force in each leg has been neglected in (16a) and (16b) so as to obtain six equations with six unknown actuating forces on the moving platform corresponding to its demanded pose variation. Of course, (10) to (15d) should also be invoked during the computation. Besides the neglected inertia, the additional effects of joint friction and the longitudinal inertia of the top part of each leg arise during the platform motion. These call for a control strategy and its performance analysis through theoretical simulation of the forward modeling.

VI. Forward Modeling with Control

The forward modeling provides the variation of the pose of the payload with time corresponding to known variations of forces imparted to it. While the force component $F_{Ti(Biz)}$ along the axis of Leg i originates from the motor,the component $F_{Ti(Bix)}$ perpendicular to it arises due to the friction and inertia [12]. Starting from the known initial conditions at the neutral, the platform pose can be determined by simple integration of

$$\dot{\mathbf{x}}_{p(o)} = \mathbf{v}_{p(o)}, \tag{22a}$$

$$\dot{\boldsymbol{\theta}}^{p}_{(o)} = \boldsymbol{\omega}^{p}_{(o)}, \tag{22b}$$

in which the linear and angular velocity of the payload can be obtained by rewriting (16a) and (16b) in terms of variables at times t and t-δt as

$$\dot{\mathbf{v}}_{p(o)} = -g\hat{k} + (1/m_p)\times \begin{Bmatrix} \sum_{i=1}^{6}\{i_{(Bix)}(t)F_{Ti(Bix)}(t) + i_{(Biz)}(t)F_{Ti(Biz)}(t)\} \\ \sum_{i=1}^{6}\{j_{(Bix)}(t)F_{Ti(Bix)}(t) + j_{(Biz)}(t)F_{Ti(Biz)}(t)\} \\ \sum_{i=1}^{6}\{k_{(Bix)}(t)F_{Ti(Bix)}(t) + k_{(Biz)}(t)F_{Ti(Biz)}(t)\} \end{Bmatrix}, \tag{22c}$$

and

$$\dot{\boldsymbol{\omega}}^{p}_{(o)} = \mathbf{R}^{T}_{p,o}(t)[\begin{Bmatrix} (I^{p}_{(py)} - I^{p}_{(pz)})\omega^{p}_{(py)}(t-\delta t)\omega^{p}_{(pz)}(t-\delta t) \\ (I^{p}_{(pz)} - I^{p}_{(px)})\omega^{p}_{(pz)}(t-\delta t)\omega^{p}_{(px)}(t-\delta t) \\ (I^{p}_{(px)} - I^{p}_{(py)})\omega^{p}_{(px)}(t-\delta t)\omega^{p}_{(py)}(t-\delta t) \end{Bmatrix} + \mathbf{x}_{Ti(p)} \times \begin{Bmatrix} \sum_{i=1}^{6}\{i_{(Bix)}(t)F_{Ti(Bix)}(t) + i_{(Biz)}(t)F_{Ti(Biz)}(t)\} \\ \sum_{i=1}^{6}\{j_{(Bix)}(t)F_{Ti(Bix)}(t) + j_{(Biz)}(t)F_{Ti(Biz)}(t)\} \\ \sum_{i=1}^{6}\{k_{(Bix)}(t)F_{Ti(Bix)}(t) + k_{(Biz)}(t)F_{Ti(Biz)}(t)\} \end{Bmatrix}]/\mathbf{I}^{p}_{(p)} \tag{22d}$$

where

$$F_{Ti(Bix)} = -(C^{u} + C^{s})\,|\,v_{Ti(Bix)}\,|\,/(l^{a}_{i})^{2} + [m^{m}(l^{m})^{2} + m^{l}\{(l^{l})^{2} + l^{l}l^{m} + (l^{m})^{2}\} + m^{u}\{3(l^{a}_{i})^{2} - 3l_{u}l^{a}_{i} + (l^{u})^{2}\}] \times a_{Ti(Bix)}/(l^{a}_{i})^{2}, \tag{23a}$$

and

$$\boldsymbol{F}_{Ti(Biz)} = \boldsymbol{F}^{(e)}_{Ti(Biz)} - \left[I^{ml}\left\{k_{(Bix)}\alpha^{p}_{(x)} + k_{(Biy)}\alpha^{p}_{(y)} + k_{(Biz)}\alpha^{p}_{(z)}\right\} + C^{s}\left|\omega^{ui}_{(Biz)}\right| + C^{b}\left|\omega^{mi}_{(Biz)}\right|\right] \div p^{b} - m^{u}a_{Ti(Biz)} + \boldsymbol{F}^{(fb)}_{Ti(Biz)}, \tag{23b}$$

in which the symbols have been used as follows – (a) C^{u}, C^{s} and C^{b} are the torque coefficients of the universal, spherical and ball-screw joints, (b) m^{m}, m^{u} and m^{l} are the masses of the motor and the upper and lower parts of each leg, (c) l^{m}, l^{u} and l^{l} are the lengths of the motor and the upper and lower parts of each leg and respectively and (d) I^{ml} is the moment of inertia of the motorized leg about its centerline.

DOI: 01.IJMMS.02.02.51

For minimizing the deviation between the demanded variation of the length $l_i^{a(d)}$ and $v_i^{a(d)}$ velocity of each leg from those estimated as $l_i^{a(e)}$ and $v_i^{a(e)}$ by a feedforward strategy, a feedback correction for the force has been considered as

$$\boldsymbol{F}_{Ti(Biz)}^{(fb)} = k_p\left(l_i^{a(d)} - l_i^{a(e)}\right) + k_D\left(v_i^{a(d)} - v_i^{a(e)}\right), \quad (23c)$$

where the proportional and derivative gains are represented by k_P and k_D respectively.

VII. CONTROL DESIGN AND PERFORMANCE ANALYSIS

In order to accomplish the design analysis, the formulation presented above has been implemented in Simulink framework. The objective of the study is to ascertain the feasibility of the proposed control for achieving different steady demands of basic displacements starting from the neutral pose of the platform in each case represented in Figs. 5 and 6. While the maximum force limit of Danahaer-motion EC2-B23-10L-5B-600 actuator for 100% duty cycle of 830N has been set as a constraint in the simulation, the values for the variables and parameters considered in the study are C^b, C^s and C^u equal to 0.001, 0.002 and 0.0001 N-m/s respectively, I^{mi} , $I^p_{(px)}$, $I^p_{(py)}$ and $I^p_{(pz)}$ equal to 1.37×10^{-6}, 86.54, 86.54 and 44.48 kg-m^2 respectively l^l , l^m , l^u and $z_{p0(o)} - z_{q0(o)}$ equal to 1.0, 0.179, 0.8 and 0.2m respectively and m^l m^m, m^u m^p equal to 3.5, 4.63 2.5 and 200kg respectively. For the numerical simulation, the proportional and derivative gains have been set as 500N/m and 120N-s/m respectively.

For the control of pure surge, sway or heave displacement, a constant feedforward target of the actuated lengths and a constant estimate of the motor torques corresponding to the target steady pose have been added to the feedback. Fig. 5 shows the predicted control performance to be quite satisfactory. No significant cross-coupled displacement has been predicted corresponding to these linear displacement demands.

Figure 6 depicts the predicted dynamics of the platform with different control strategies employed for attaining two different angular displacement demands. Figs. 6 (a) to (c) pertain to a 15^0 demand of roll, Figs. 6 (d) to (f) correspond to a 10^0 demand of pitch and the strategies have been numbered in each figure as 1 to 5. Case 1 shows the predicted dynamics, when the desired displacement has been applied as a simple step demand.

Though the basic demand can be seen as achieved by about 1s, it is associated with cross-coupled steady-state displacement errors in both horizontal and vertical directions. In cases of roll and pitch demands, the coupled horizontal errors per degree of the angular displacement have been predicted as –3.5mm in sway and 3.5mm in surge respectively. The corresponding heave errors are –0.5mm/^{0} and –0.3mm/^{0} respectively.In each of Figs. 6 (a) to (f), Case 2 depicts the predicted dynamics when besides raising the basic demand as a simple step in roll or pitch, compensating step demands of linear displacement have been added. The objective is to mitigate the steady-state errors that have been predicted to arise in Case 1 by putting compensating demands as 51.7mm sway and 7.1mm heave for 15^0 roll and -34.6mm surge and 3.0mm heave for 10^0 pitch. Figs. 6(a) and (d) show that the basic dynamics for Cases 1 and 2 to be identical, whereas the predicted cross-coupled displacements in Figs. 6 (b), (c), (e) and (f) corresponding to Case 2 can be seen to be negligible in the steady-state and quite small even during the transients.

Cases 3 to 5 of Figs. 6(a) and 6(c) reveal identical dynamics for the demanded basic poses, if either the roll or the pitch is applied as 10^0/s ramp demand for 1.5s or 1s respectively. Case 3 correspond to the dynamics corresponding to this tracking of the ramp demand is placed without any compensation, the variations of the cross-coupled displacement errors can be seen to be given by Case 3 is each of Figs. 6 (b), (c), (e) and (f).

Though the predicted transient variations between Cases 1 and 3 are different, the steady-state errors are almost equal. In Cases 2 and 4, identical compensating demands have been employed for mitigating the cross-coupled linear displacement errors. In both the cases, negligible steady-state errors have been predicted. However, the transient errors for Cases 2 and 4 have been found as negligible and significant respectively.

For Case 5, the compensations have been applied in rate forms as 34.5mm/s sway and 4.7mm/s heave for roll demand of 10^0/s over a period of 1.5s and -34.5mm/s surge and 3.0mm/s heave for pitch demand of 10^0/s over a period of 1.0s. Figs. 6 (b), (c), (e) and (f) for this case show only about 1.5mm and 0.75mm maximum transient cross-coupled heaves during roll and pitch dynamics respectively. Thus, a ramp demand of an angular displacement should be associated with compensation in the form of rates.

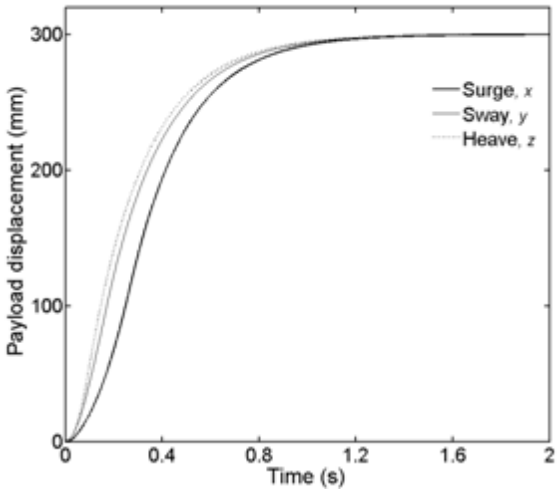

Figure 5. Payload dynamics in surge, sway and heave for respective step demands

DOI: 01.IJMMS.02.02.51

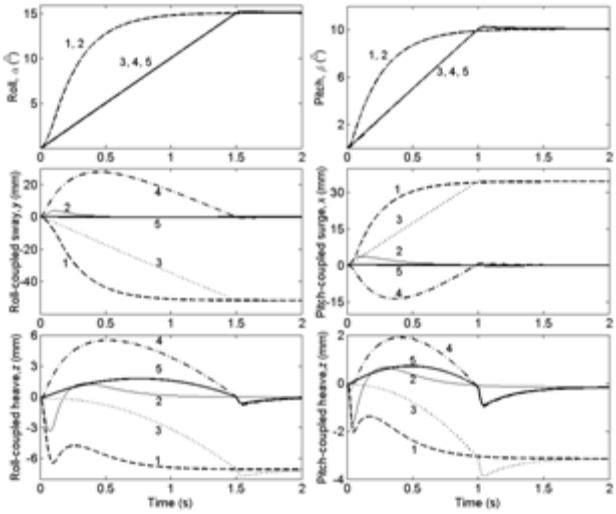

Figure6. Transient variations of (a) roll with (b) coupled sway and (c) coupled heave for 15^0 final demand and (d) pitch with (e) coupled surge and (f) coupled heave for 10^0 final demand for different control strategies – 1: only step demand, 2: step demand with step correction, 3: only 10^0/s rate demand, 4: 10^0/s rate demand with step correction and 5: 10^0/s rate demand with linear displacement correction as rates.

Conclusions

A control-integrated six degree-of-freedom Stewart platform with torque-motor operated six ball-screw actuators has been designed. Both the inverse and the forward modeling involving active rotation in the ball-screw actuators have been accomplished. Simulink implementation of these models has provided the sizing as well as control design of the system.

A two-dimensional simultaneous step-by-step search has been executed for a given payload size and range of its demanded pose and the rates, along with the constraints of the permissible maximum joint angles and available actuation capabilities in terms of stroke, force, velocity and acceleration limits. Control structures have been suggested for achieving any displacement demand in surge, sway, heave, roll or pitch with minimal cross-coupled dynamics. A PD feedback structure has been integrated with the model-based feedforward estimates for all the cases. For the angular

Acknowledgment

We sincerely acknowledge RCI Hyderabad, India for a collaborating work with them and CSIR, New Delhi, India for the scholarship support.

References

[1] D. Stewart, "A platform with six degrees of freedom", Proceedings of Institute of Mechanical Engineering 180 (1) (1965) pp. 371–386.

[2] K. Liu, J. Fitzgerald, F.L. Lewis, "Kinematic analysis of a Stewart platform manipulator", *IEEE Transactions on Industrial Electronics*, 40 (2) 1993) pp. 282–293.

[3] J.-P. Merlet, "Direct kinematics of parallel manipulators", *IEEE Transactions on Robotics and Automation*, 9 (6) (1993) pp. 842-845.

[4] E.F. Fichter, "A Stewart platform-based manipulator: general theory and practical construction", *International Journal of Robotics Research*, 5 (2) (1986) pp. 157–82.

[5] B. Dasgupta, T.S. Mruthyunjaya, "Closed-form dynamic equations of the general Stewart platform through the Newton–Euler approach", *Mechanisms ane Machines Theory* 33 (7) (1998) pp. 993–1012.

[6] B. Dasgupta, T.S. Mruthyunjaya, "A Newton–Euler formulation for the inverse dynamics of the Stewart platform manipulator", *Mechanisms and Machines Theory* 33 (7) (1998) pp. 1135–1152.

[7] M. Raghavan, "The Stewart platform of general geometry has 40 configurations", *Journal of Mechanical Design*, 115 (1993) pp.277-282.

[8] C. Yang, Q. Huang, H. Jiang, O. Ogbobe Peter, J. Han, "PD control with gravity compensation for hydraulic 6-DOF parallel manipulator", *Mechanisms and Machines Theory* 45 (7) (2010) pp. 666–677.

[9]N. Andreff, P. Martinet, Unifying kinematic modeling, identification, and control of a Gough–Stewart parallel robot into a vision-based framework, *IEEE Transactions on Robotics and Automation*, 22 (6) (2006) pp.1077-1086.

[10] O. Tahri, Y. Mezouar, N. Andreff, P. Martinet, Omnidirectional visual-servo of a Gough–Stewart platform, *IEEE Transactions on Robotics and Automation*, 25 (1) (2009) pp.178-183.

[11] M.D. Shuster, "Spacecraft attitude determination and control", Chapter 5 in V.L. Pisacane and R.C. Moore (eds.), *Fundamentals of Space Systems*, Oxford University Press, 1994, pp. 245–336.

[12] P. Hamon, M. Gautier, P. Garrec, A. Janot, "Dynamic Identification of Robot with a Load Dependent Joint Friction Model", in *Proc. IEEE Conference on Robotics, Automation and Mechatronics*, 2010, pp. 129-135.

DOI: 01.IJMMS.02.02.51